Metrol. Meas. Syst., Vol. 28 (2021) No. 2, pp. 357–370
DOI: 10.24425/mms.2021.136612

PAN POLSKA AKADEMIA NAUK

METROLOGY AND MEASUREMENT SYSTEMS
Index 330930, ISSN 0860-8229
www.metrology.wat.edu.pl

M&MS

NEW APPROACH TO SPINDLE THERMAL EXTENSION MEASURING BASED ON MACHINE VISION FOR THE VERTICAL MACHING CENTRE

Dongxu Su, Xin Cai, Yang Li, Wanhuan Zhao, Huijie Zhang

Xi'an Jiaotong University, State Key Laboratory for Manufacturing System Engineering, Xi'an, Shaanxi 710054, China
(*sdx1994527@stu.xjtu.edu.cn*, *caixin@stu.xjtu.edu.cn*, *liyangxx@stu.xjtu.edu.cn*, ✉ *13020367155@163.com*,
+86 029 8339 9520, *zhj@163.com*)

Abstract

When machine tool spindles are running at a high rotation speed, thermal deformation will be introduced due to the generation of large amounts of heat, and machining accuracy will be influenced as a result, which is a generalized issue in numerous industries. In this paper, a new approach based on machine vision is presented for measurements of spindle thermal error. The measuring system is composed of a Complementary Metal-Oxide-Semiconductor (CMOS) camera, a backlight source and a PC. Images are captured at different rotation angles during end milling process. Meanwhile, the Canny edge detection and Gaussian sub-pixel fitting methods are applied to obtain the bottom edge of the end mill which is then used to calculate the lowest point coordinate of the tool. Finally, thermal extension of the spindle is obtained according to the change of the lowest point at different time steps of the machining process. This method is validated through comparison with experimental results from capacitive displacement sensors. Moreover, spindle thermal extension during the processing can be precisely measured and used for compensation in order to improve machining accuracy through the proposed method.

Keywords: Spindle thermal extension measuring, machine vision, Gaussian sub-pixel fitting, thermal error compensation.

1. Introduction

The machine tool spindle is the core component to ensure the machining accuracy and efficiency [1, 2]. When the spindle is running at high rotation speeds, a large amount of heat is generated due to bearing friction and power loss of the motor. If the heat cannot be dissipated in time, thermal extension of spindles and dimensional deviation of machined components will be induced by temperature rise. Accurate measurement of spindle thermal extension is the basis for spindle thermal error modelling and compensation. Currently, eddy current and capacitive sensors are the most widely used to measure the thermal error of the spindle [3]. Liu [4] used a standard mandrel mounted on the spindle and eddy current sensors to measure the spindle thermal error.

Article history: received September 8, 2020; revised November 24, 2020; accepted January 18, 2021; available online March 19, 2021.

In the test, standard mandrel was mounted on the spindle and the eddy current displacement sensors were arranged around the mandrel. When the spindle was rotating, signals could be captured by sensors. And the spindle thermal error was calculated from the distance variation between the mandrel and the sensor at different time steps. Similarly, Moriwaki *et al.* [5] and Li *et al.* [6] used capacitive displacement sensors to measure the spindle thermal error. Meanwhile, the dial indicator [7] and the ball bar [8] were also applied to measure the spindle thermal error, however, these are not widely used methods due to low accuracy. The methods above can be performed only under a non-cutting, no-load condition, as installation of a standard mandrel on the spindle is always required for all of them. However, heat generation of thew bearing and the spindle motor will be significantly increased due to cutting loads, which will lead to a larger spindle thermal error in actual machining process. Furthermore, the non-contact laser light barrier system [9] is also widely used in the measurements of spindle thermal deformation on-line by calculating coordinate differences of the *tool central point* (TCP) in the machine tool coordinate system. However, high requirements for positioning accuracy and repeat positioning accuracy of the machine tool are essential for this approach, which also needs a more open CNC system to provide machine coordinate values in order to perform calculations. In result, implementation of this method in actual machining process is not reasonable for both economic and operating reasons.

Therefore, a more generalized method with simple operations and less accessories is still required for measuring the spindle thermal error under actual processing conditions. Recently, *machine vision* (MV) based techniques are widely used in industries. Jurkovic *et al.* [10], Dai and Zhu [11] used vision systems to measure tool wear in turning and micro-milling, respectively. Moreover, Wang *et al.* [12] proposed a method based on MV for detecting the depth dimension error of a part cavity. Based on the edge extraction method, Kavitha and Ashok [13] analyzed the radial runout of the lathe spindle.

In this paper, a novel method is proposed to measure spindle thermal extension using vision system. The standard mandrel is not required for this approach, which can be applied in actual processing. In order to improve measurement accuracy, the Gaussian fitting sub-pixel edge extraction method is applied for image processing. This method was validated through comparison against experimental data obtained by the capacitive displacement sensor. In addition, good performance of on-line measurement based on the current method is also obtained through cutting tests. The testing results can be used to compensate the axial thermal error of the spindle and improve the workpiece dimensional accuracy.

2. Development of a vision system for spindle thermal extension measuring

In order to measure spindle thermal extension during processing, direct identification of cutting tools from captured images is essential. Within the whole machine tool system, the tool tip can be regarded as the terminal point which has a direct contact with the workpiece, as a result, spindle thermal deformation induced position alterations will directly affect the machining accuracy. Meanwhile, the point of the tool tip, which is the lowest point in the Z direction of the *Vertical Machining Center* (VMC), is easier to identify from the image. Thus, the tool tip points are used as marking points, and spindle thermal extension ΔL is measured by the vertical position change in the image, as shown in Fig. 1.

Sspindle thermal extension during processing is generally from tens of microns to hundreds of microns. Therefore, high-resolution cameras and suitable *Light Emitting Diode* (LED) light sources are both essential for obtaining high-quality images with clear boundaries.

Metrol. Meas. Syst., Vol. 28 (2021), No. 2, pp. 357–370
DOI: 10.24425/mms.2021.136612

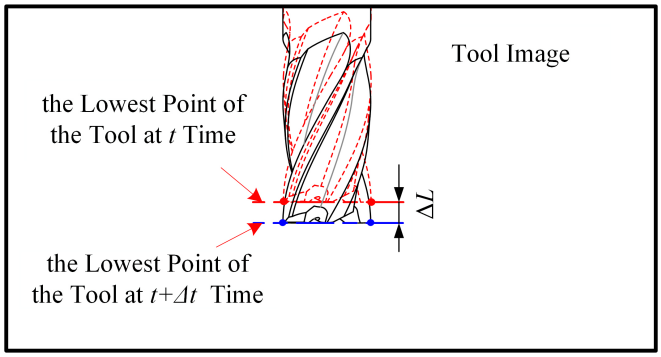

Fig. 1. Schematic of spindle thermal extension measurement.

2.1. Composition of measurement system

The vision system for measuring spindle thermal extension is shown in Fig. 2. It is composed of a CMOS camera (model: Basler ace acA4024-29um), a lens (model: M0824 MPW2), a backlight source and a PC, and image processing programs developed by Python are used to obtain spindle thermal extension.

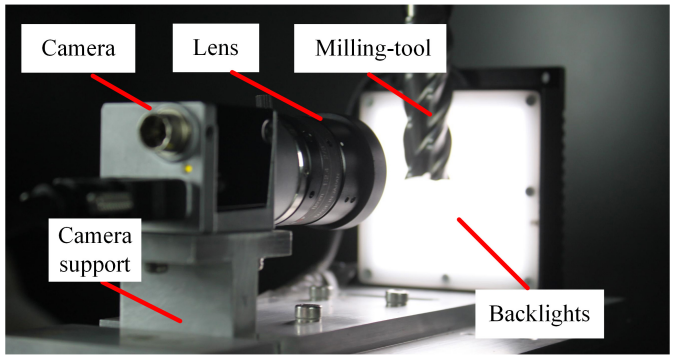

Fig. 2. Measuring device for spindle thermal extension measurement using the vision system.

The relevant parameters of the camera are shown in Table 1. In order to improve the measurement accuracy of the camera, M0824 MPW2 lens with parameters shown in Table 2 is selected.

Table 1. Main parameters of Basler Ace acA4024-29um camera.

Sensor Type	Resolution (H × V)	Pixel Size (H × V)	Frame Rate	Lens Mount
CMOS	4024 px ×3036 px	1.85 μm ×1.85 μm	31 fps	C-mount

Table 2. Main parameters of lens M0824 MPW2.

Sensor Compatibility	Focal Length (mm)	Aperture	Lens Mount	Dimensions (ø × L)
2/3	8	F2.4 ~F16.0	C-mount	Φ 32 × 45.71

Because the profile of the spiral end mill is complicated, and the surface coating of the tool will significantly affect the imaging quality, a white backlight source is placed on the rear side of the spindle to obtain images with a bright background and a dark foreground, in which the tool edges are shaper. Based on this method, surface information on the end mill is weakened, however, the contour of the tool can be significantly improved, which can simultaneously reduce the complexity of the image processing program and ensure the stability of the measurement.

Moreover, a protective device is designed to avoid the influences of chips and cutting fluid on image quality, as shown in Fig. 3. The camera and backlights are housed in the protective covering. The sliding door, controlled by the stepper motor, is closed during machining in order to prevent the entrance of chip and cutting fluid, while it is open during the measurement.

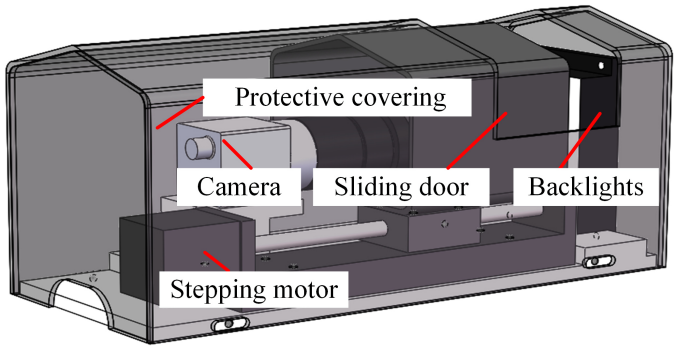

Fig. 3. Protection device the for visual measurement system.

The entire measurement work is divided into the following steps: a) camera calibration, b) set-up of parameters and image acquisition, c) image processing.

2.2. Camera calibration

Camera calibration is the essential part of visual measurement. The relationship between a single pixel and its actual length can be obtained from this step. The standard checkerboard calibration template is adopted in the present work. It is fixed on the spindle by connecting plate. The calibration plate image with clear boundary is obtained using a white dome light source, as shown in Fig. 4.

The number of pixels in the XY direction of each square in the image can be calculated through image processing methods. Then, the actual length represented by each pixel in the image is calculated as follows:

$$P_x = \frac{\sum_{i=1}^{N} \frac{d}{num_{p\_x}}}{N}, \tag{1}$$

$$P_y = \frac{\sum_{i=1}^{M} \frac{d}{num_{p\_y}}}{M}, \tag{2}$$

Metrol. Meas. Syst., Vol. 28 (2021), No. 2, pp. 357–370
DOI: 10.24425/mms.2021.136612

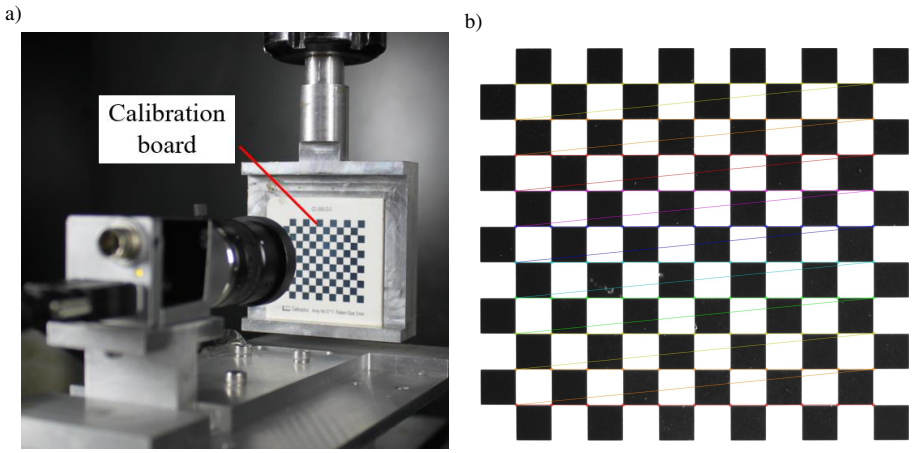

Fig. 4. Camera calibration. Calibration board installation position (a). Calibration board image (b).

where, d is the actual size of each checkerboard. M, N are both checkerboard ranks. num_{p_x}, num_{p_y} are numbers of pixels per square. A standard square calibration board of 33×30 mm (the size of each square is 3×3 mm, with 11 rows and 10 columns) is used in this paper. Once the identification of the checkerboard corner points in the image is finished and their pixel coordinates are obtained, the actual size represented by each pixel point can be calculated as 13.56 μm in this study.

2.3. Camera parameter setting and image acquisition

The testing subject needs to be placed between the camera and the light source when the backlight light source is used. Therefore, the spindle is located between the camera and the light source during the measurement process and its height needs to be adjusted in order to guarantee that the bottom edge of the tool is within the central part of the image. Then, a clear tool image can be captured by adjusting the object distance, aperture size and light source intensity. Because there are multiple flutes in the end mill, it is hard to capture the coordinate information for each tip point of the tool based on a single tool image. Therefore, it is necessary to capture a series of images at different angles of the tool to obtain position coordinate information on each point of the tool by setting a reasonable spindle speed and sampling frequency. In this process, a reasonable exposure time also should be set so that a clear and shadow-free tool image can be obtained when the spindle is rotating. Spindle speed and camera sampling frequency can be given by:

$$n = \frac{\alpha \cdot f}{360} \times 60, \tag{3}$$

where n is spindle speed (r/min), f is frame rate (fps), α is the angle at which the tool rotates every frame ($^\circ/f$). In this paper, exposure time is set as 200 μs, $\alpha 15^\circ/f$, and f 20 fps. Spindle speed n can be calculated as 50 r/min. Figure 5 shows a series of images acquired during the test.

Fig. 5. A sequence of end mill images acquired at the spindle speed of 50 r/min.

3. Measurement algorithm

To improve measurement accuracy, sub-pixel boundary extraction methods based on pixel-level boundary extraction approach are always adopted. Interpolation [14,15], moment estimation [16–18] and fitting [19–21] are the most common methods used in sub-pixel extraction. The image processing algorithm adopted in this paper is shown in Fig. 6. The Canny edge extraction method is applied to locate the tool bottom edge at first. Then the Gaussian fitting sub-pixel boundary extraction method is used to obtain the sub-pixel coordinates of the tool bottom edge. Finally, the coordinates of the tool tip point in each frame of the tool image are extracted to calculate the coordinate values at the tool tip point of the end mill. Then spindle thermal extension during processing can be obtained according to the change of the ordinate value of this point at different time steps.

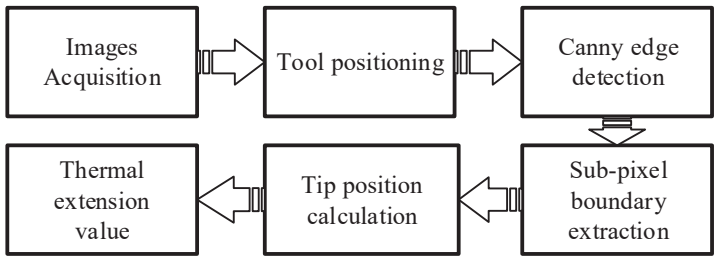

Fig. 6. Image processing algorithm flowchart.

3.1. Canny edge extraction method

Canny edge detector [22] is a commonly used edge detection method [23], where the magnitude image and gradient image are calculated with (4) and (5) after Gaussian filtering as:

$$M(x,y) = \sqrt{g_x^2 + g_y^2}, \tag{4}$$

$$\alpha(x,y) = \arctan\left[\frac{g_y}{g_x}\right], \tag{5}$$

where: $g_x = \partial f_x/\partial x$, $g_y = \partial f_y/\partial y$, g_x, g_y are the gradient values of the image in the X and Y directions, respectively. After applying non-maximum suppression to the gradient image,

thresholds TH and TL are set to get image $g_N(x, y)$ as followings:

$$\begin{aligned} g_{NH}(x, y) &= g_N(x, y) \geq TH \\ g_{NL}(x, y) &= g_N(x, y) \geq TL \end{aligned}, \tag{6}$$

$$g_N(x, y) = g_{NL}(x, y) - g_{NH}(x, y), \tag{7}$$

where: $g_N(x, y)$ is the image obtained by non-maximum suppression. TH is the higher threshold, while TL is the lower one. The tool edge image obtained with the Canny edge extraction method is shown in Fig. 7.

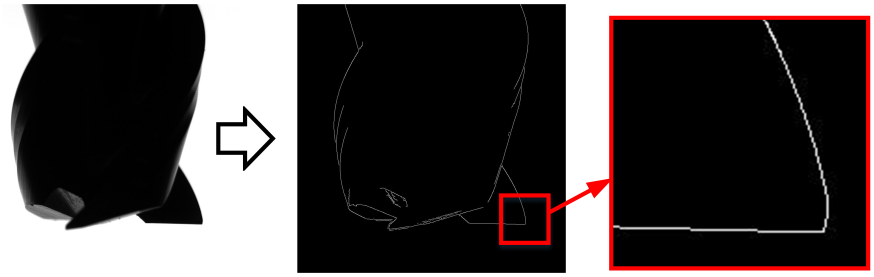

Fig. 7. The tool edge image obtained by the Canny edge extraction method.

3.2. Gaussian fitting sub-pixel edge extraction method

In the course of image acquisition, the CMOS sensor's response to the step edge is a gradual change (from light to dark or dark to light), which is shown in Fig. 8. Near the edge of the tool image, the grayscale difference value of the pixels is similar to Gauss distribution, as shown in Fig. 9.

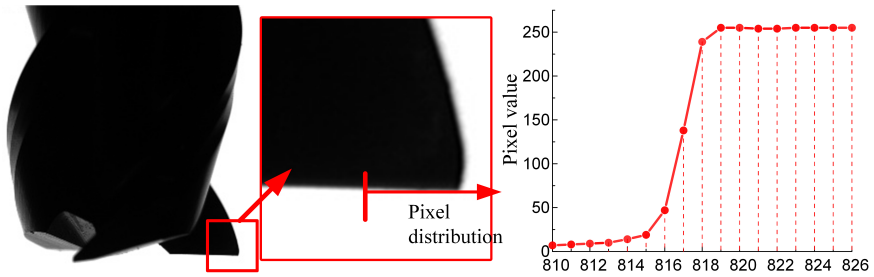

Fig. 8. Pixel value distribution at the edges in the actual tool image.

Therefore, the Gaussian function is used to fit pixel gradient values according to following the equation:

$$y = \frac{1}{\sqrt{2\pi}\sigma} \exp\left(-\frac{(x-\mu)^2}{2\sigma^2}\right), \tag{8}$$

where: μ is mean value, σ is standard deviation. The extreme coordinates of the Gaussian function are the sub-pixel edge points. To simplify calculation, five points of (x_i, y_i) including the point where the difference is the largest and two points on each of its sides, are selected to fit the

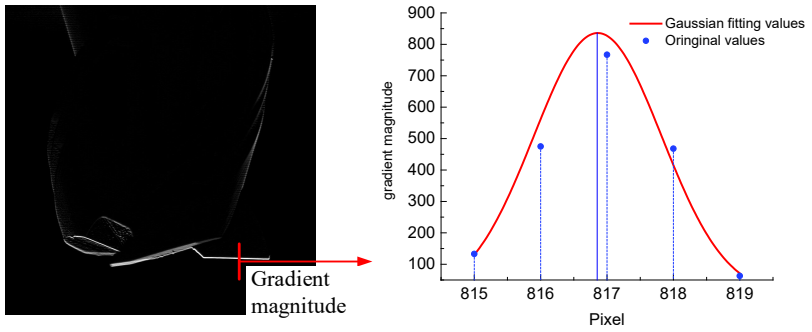

Fig. 9. Gaussian distribution of edges in gradient images.

Gaussian curve in total. With application of the natural logarithm on both sides of equation (8), Equation (9) is obtained based on the Square Aperture Sampling Theorem.

$$y_i' = \int_{i-0.5}^{i+0.5} \left(ax^2 + bx + c\right) \mathrm{d}x, \tag{9}$$

where: $y_i' = \ln y_i$, $i = -2, -1, 0, 1, 2$.

The matrix form of (9) is given as follows:

$$K \cdot P = B, \tag{10}$$

$$K = \begin{bmatrix} \frac{49}{12} & \frac{13}{12} & \frac{1}{12} & \frac{13}{12} & \frac{49}{12} \\ -2 & -1 & 0 & 1 & 2 \\ 1 & 1 & 1 & 1 & 1 \end{bmatrix}^T, \quad P = \begin{bmatrix} a & b & c \end{bmatrix}^T, \quad B = \begin{bmatrix} \ln(y_{-2} + M) \\ \ln(y_{-1} + M) \\ \ln(y_0 + M) \\ \ln(y_1 + M) \\ \ln(y_2 + M) \end{bmatrix}.$$

With solution of the linear equations above, the extreme coordinates x' of the fitted curve can be obtained as:

$$x' = -\frac{b}{2a}. \tag{11}$$

The sub-pixel coordinate value $x_{\text{sub\_pixel}}$ of the bottom edge of the tool can be calculated:

$$x_{\text{sub\_pixel}} = x_0 + x', \tag{12}$$

where, x_0 is the pixel-level edge coordinates in the image.

3.3. Calculation of tool tip point coordinates

Through the calculation of sub-pixel coordinates of the tool bottom edge in the i-th image, a series of coordinate points $\left(x_{i\_j}^t, y_{i\_j}^t\right)$ of the tool bottom edge at time t are obtained. The ordinate value at the position of the tool tip point is the largest in the image, which means that

the coordinate $\left(x^t_{i\_j}, y^t_{i\_\max}\right)$ is the desired tool tip point in the image. Meanwhile, to avoid the interference induced by noisy points, the first N_{avg} coordinate points with larger ordinate values are extracted and their average value is calculated as the position of the tool tip point in the current frame. The stability of measurements will be significantly improved with the increase of points. Correspondingly, the measured value might be slightly smaller than the actual value. N_{avg} is taken as 10 in the present work.

$$\overline{y}^t_{i\_\max} = \frac{\sum_{j=1}^{N_{avg}} y^t_{i\_j}}{N_{avg}}, \tag{13}$$

where: $\left(x^t_{i\_j}, y^t_{i\_j}\right)$ are the coordinates of the j-th point of the tool bottom edge in the *i-th* frame measured at time t. $\overline{y}^t_{i\_\max}$ is the vertical coordinate value of the tool tip point in the *i-th* frame measured at time t. The largest ordinate value $y^t_{\max}$ among the total N images is the position of the tool tip point at time t,

$$y^t_{\max} = \max\left\{\overline{y}^t_{i\_\max} \middle| \, i = 1, 2, 3, \ldots, N\right\}. \tag{14}$$

Then spindle thermal extension ΔL during the time period $(t, t + \Delta t)$ can be calculated as follows:

$$\Delta L = P_y \cdot \left(y^{t+\Delta t}_{\max} - y^t_{\max}\right). \tag{15}$$

4. Application in processing

4.1. Measurement accuracy validation

Thermal spindle extension was experimentally measured using the proposed method in this paper for validating purposes. Then the measurement results were compared with the results obtained through the displacement sensor. The displacement sensors were installed in accordance with ISO 230-3 as shown in Fig. 10. Meanwhile, two Pt100 temperature sensors were arranged to measure spindle and environment temperature, the location of which are shown in Fig. 11. A five-axis *vertical machining center* (VMC) adopting the Heidenhein system was used in the experiment. At the ambient temperature of 23°C the positioning accuracy of its Z axis was 8.98 μm with repeat positioning accuracy 4.61 μm which was measured by the laser interferometer according to the ISO230-2.

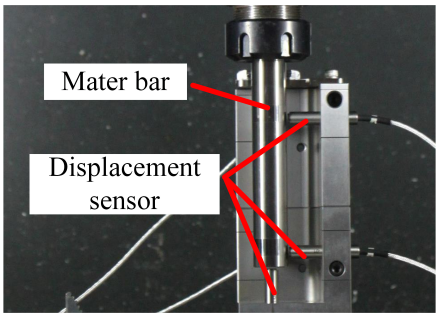

Fig. 10. Displacement sensor arrangement.

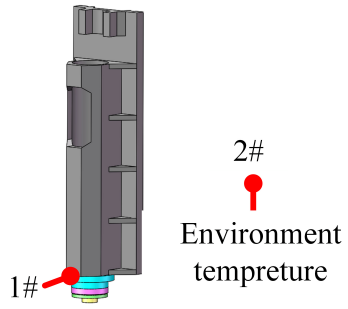

Fig. 11. Location of the temperature sensor.

During the experiment, the spindle had been running at 8000 r/min until the thermal steady state was reached. The spindle temperature rise was recorded by the temperature sensors, as shown in Fig. 12. It illustrates that the environment temperature was kept at 23°C and the temperature rise at the front of the spindle was about 12°C.

Spindle thermal extension during operation was measured by the vision system and displacement sensors, respectively. The measurement results of these two methods are shown in Fig. 13. It illustrates that measurement error of vision system can be controlled within 5 microns throughout the process. It also verifies that accurate measurement results can be obtained by the method proposed in this paper.

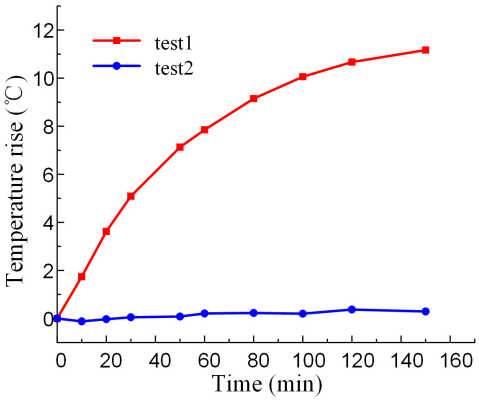

Fig. 12. Spindle temperature rise at 8000 r/min.

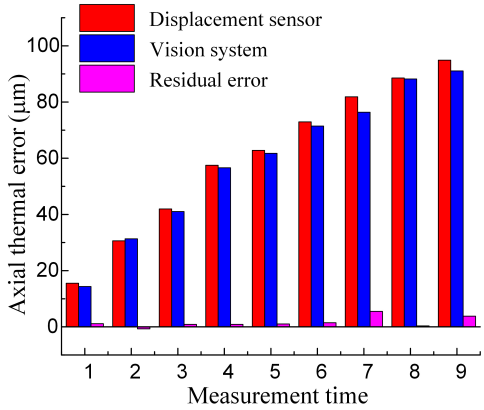

Fig. 13. Comparison of measurement results.

4.2. Z-direction zero correction during processing

Samples were designed as shown in Fig. 14 in order to validate the proposed method, which were machined in the same VMC as the previous experiment to prove same boundary conditions. The vision system was fixed on the left side of the VMC table, as shown in Fig. 15.

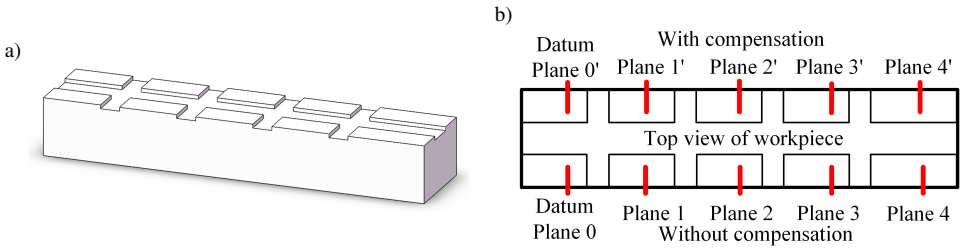

Fig. 14. Experimental sample. (a) 3D model of experimental sample, (b) the planes to be machined.

During the experiment, the Datum Plane 0 shown as Fig. 12 was machined first. Then spindle was idling at 6000 r/min for 20 min to make the temperature increase. And then Plane 1 was machined at the same Z position without any compensation. Similarly, planes 2, 3 and 4 were machined at intervals of 30 min, 30 min, and 40 min, respectively, without compensation.

When the spindle was cooled down to room temperature, the Datum Plane 0′ was machined. After idling at 6000 r/min for 20 min, the spindle was moved to the left measurement position to

Metrol. Meas. Syst., Vol. 28 (2021), No. 2, pp. 357–370
DOI: 10.24425/mms.2021.136612

measure spindle thermal extension. By correcting the Z coordinate value in the G54 coordinate system of the VMC, the spindle thermal extension value was compensated. And then Plane 1′ was machined with the compensation. Similarly, Plane 2′, 3′ and 4′ were processed in sequence at intervals of 30 min, 30 min, and 40 min with compensation, respectively. In this test, a flat-bottom end mill with a diameter of 10 mm was used. The cutting depth was 1mm, and the cutting width was 5 mm. The feed rate was 1000 mm/min. The distance between each plane and the datum plane is measured by a three-coordinate measuring instrument, as shown in Fig. 16. And the experiment was performed three times in order to prove the repeatability.

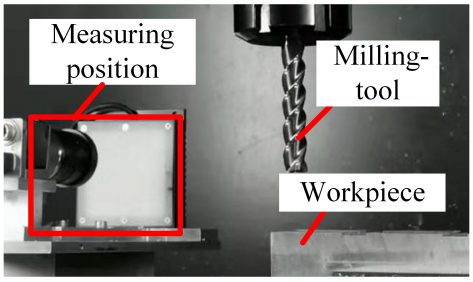

Fig. 15. Vision system installation position.

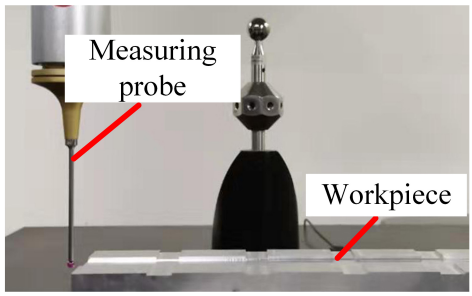

Fig. 16. Part dimensions measuring.

The spindle temperature rise was up to 7°C within 2 hours, as shown in Fig. 17. The machining accuracy measurement results are shown in Fig. 18. Without compensation, the dimensional deviation along the Z direction Z of the part caused by spindle thermal extension within 2 hours increases up to 46 μm. After the repeated measurements and compensation of spindle thermal extension with the proposed method, the dimensional accuracy is significantly improved, and the error can be limited to less than 5 μm every time. It is concluded that the proposed method can accurately measure spindle thermal extension during processing and the dimensional deviation caused by this extension can be effectively reduced with the online compensation in the Z direction of the machine tool.

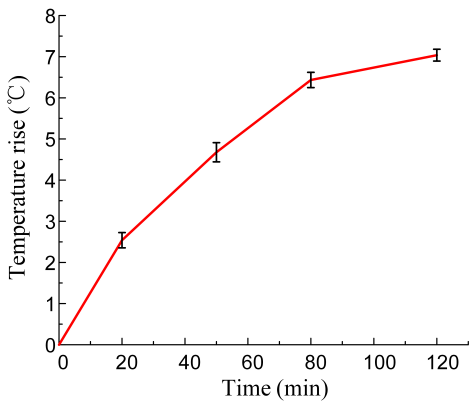

Fig. 17. Temperature rise at 6000 r/min.

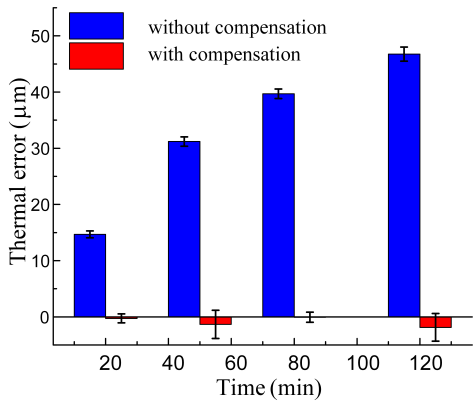

Fig. 18. Experimental sample dimensional deviation.

5. Conclusions

Machining accuracy of components can be significantly influenced by spindle thermal extension. In order to develop an online measuring method to obtain the extension data during machining, a novel approach based on MV method is proposed in this paper. The Canny edge detector and Gaussian sub-pixel fitting method are used to identify the lowest point at the bottom edge of the end mill. By calculating the change of the vertical coordinate value of the tool tip point, spindle thermal extension is obtained.

The machine vision method proposed in this paper is validated through comparison with the experimental results from capacitive displacement sensors. Moreover, spindle thermal extension during the processing can be precisely measured and used for compensation to decrease machining error through the proposed method. During repeat cutting tests, the dimensional deviation of the sample in the Z direction is reduced by 80%, which verifies that the proposed method can be used to improve the dimension accuracy of the workpiece effectively.

Although the protective device is adopted, the chips and cutting fluid can still affect image quality. Meanwhile, because of the curve cutting edge and the secondary flank, determining the tool boundary in the image is very complicated, which leads to a decrease in the effect of the sub-pixel algorithm. The image processing algorithms should be further improved to ensure stability and reliability of the vision system during processing.

Additionally, the deformation of the workpiece during processing is also an important part of machining errors. However, the error is difficult to be measured because of its being smaller than spindle thermal deformation. Thus, the two-scale fractal theory will be used in the subsequent research on the measurement of workpiece deformation.

References

[1] Khan, A. (2020). Experimental Study of the Heat Transfer Enhancement in Concentric Tubes With Spherical and Pyramidal Protrusions. *Journal of Applied and Computational Mechanics*, *6*(4), 801–812. https://doi.org/10.22055/jacm.2019.30122.1686

[2] Sarhan, A. A. D. (2014). Investigate the spindle errors motions from thermal change for high-precision CNC machining capability. *The International Journal of Advanced Manufacturing Technology*, *70*(5–8), 957–963. https://doi.org/10.1007/s00170-013-5339-5

[3] Li, Y., Zhao, W., Lan, S., Ni, J., Wu, W., & Lu, B. (2015). A review on spindle thermal error compensation in machine tools. *International Journal of Machine Tools and Manufacture*, *95*, 20–38. https://doi.org/10.1016/j.ijmachtools.2015.04.008

[4] Liu, T., Gao, W., Zhang, D., Zhang, Y., Chang, W., Liang, C., & Tian, Y. (2017). Analytical Modeling for Thermal Errors of Motorized Spindle Unit. *International Journal of Machine Tools & Manufacture*, *112*, 53–70. https://doi.org/10.1016/j.ijmachtools.2016.09.008

[5] Moriwaki, T., & Shamoto, E. (1998). Analysis of Thermal Deformation of an Ultraprecision Air Spindle System. *CIRP Annals-Manufacturing Technology*, *47*(1), 315–319. https://doi.org/10.1016/S0007-8506(07)62841-8

[6] Li, Y., Zhao, W., Wu, W., & Lu, B. (2017). Boundary conditions optimization of spindle thermal error analysis and thermal key points selection based on inverse heat conduction. *The International Journal of Advanced Manufacturing Technology*, *90*(9–12), 2803–2812. https://doi.org/10.1007/s00170-016-9594-0

[7] Li, T., Li, F., Jiang, Y., Zhang, J., & Wang, H. (2017). Kinematic calibration of a 3-P(Pa)S parallel-type spindle head considering the thermal error. *Mechatronics*, *43*, 86–98. https://doi.org/j.mechatronics.2017.03.002

[8] Srinivasa, N., Ziegert, J. C., & Mize, C. D. (1996). Spindle thermal drift measurement using the laser ball bar. *Precision Engineering*, *18*(2), 118–128. https://doi.org/10.1016/0141-6359(95)00053-4

[9] Ibaraki, S., Inui, H., Hong, C., Nishikawa, S., & Shimoike, M. (2019). On-machine identification of rotary axis location errors under thermal influence by spindle rotation. *Precision Engineering*, *55*, 42–47. https://doi.org/10.1016/j.precisioneng.2018.08.005

[10] Jurkovic, J., Korosec, M., & Kopac, J. (2005). New approach in tool wear measuring technique using CCD vision system. *International Journal of Machine Tools and Manufacture*, *45*(9), 1023–1030. https://doi.org/10.1016/j.ijmachtools.2004.11.030

[11] Dai, Y., & Zhu, K. (2017). A machine vision system for micro-milling tool condition monitoring. *Precision Engineering*, *52*, S780782625. https://doi.org/10.1016/j.precisioneng.2017.12.006

[12] Wang, S. M., Yu, H. J., Liu, S. H., & Chen, D. F. (2011). An on-machine and vision-based depth-error measurement method for micro machine tools. *International Journal of Precision Engineering & Manufacturing*, *12*(6), 1071–1077. https://doi.org/10.1007/s12541-011-0143-3

[13] Kavitha, C., & Ashok, S. D. (2017). A New Approach to Spindle Radial Error Evaluation Using a Machine Vision System. *Metrology and Measurement Systems*, *24*(1), 201–219. https://doi.org/10.1515/mms-2017-0018

[14] Overington, I., & Greenway, P. (1987). Practical first-difference edge detection with subpixel accuracy. *Image & Vision Computing*, *5*(3), 217–224. https://doi.org/10.1016/0262-8856(87)90052-7

[15] Tabbone, S., & Ziou, D. (1992). Subpixel positioning of edges for first and second order operators. *11th IAPR International Conference on Pattern Recognition. Vol. III. Conference C: Image, Speech and Signal Analysis*, Netherlands. https://doi.org/10.1109/ICPR.1992.202071

[16] Lyvers, E. P., Mitchell, O. R., Akey, M. L., & Reeves, A. P. (1989). Subpixel Measurement Using a Moment-Based Edge Operator. *IEEE Transactions on Pattern Analysis and Machine Intelligence*, *11*(12), 1293–1309. https://doi.org/10.1109/34.41367

[17] Tabatabai, A. J., & Mitchell, O. R. (1984). Edge location to subpixel values in digital imagery. *IEEE Transactions on Pattern Analysis & Machine Intelligence*, *PAMI-6*(2), 188–201. https://doi.org/10.1109/TPAMI.1984.4767502

[18] Yu, W., Ma, Y., Wu, X., & Liu, K. (2015). Research of improved subpixel edge detection algorithm using Zernike moments. *Chinese Automation Congress (CAC)*, China, 712–716. https://doi.org/10.1109/CAC.2015.7382590

[19] Nalwa, V. S., & Binford, T. O. (1986). On detecting edges. *IEEE Transactions on Pattern Analysis & Machine Intelligence*, PAMI-8(6), 699–714. https://doi.org/10.1109/TPAMI.1986.4767852

[20] Su, C. Y., Yu, L. A., & Chen, N. K. (2016). Effective subpixel edge detection for LED probes. *IEEE International Conference on Systems, Man, and Cybernetics (SMC),* Hungary, 000379-000382. https://doi.org/10.1109/SMC.2016.7844270

[21] Ye, J., Fu, G., & Poudel, U. P. (2005). High-accuracy edge detection with blurred edge model. *Image and Vision Computing*, *23*(5), 453–467. https://doi.org/10.1016/j.imavis.2004.07.007

[22] Canny, J. (1986). A computational approach to edge detection. *IEEE Transactions on Pattern Analysis & Machine Intelligence*, *PAMI-8*(6), 679–698. https://doi.org/10.1016/B978-0-08-051581-6.50024-6

[23] Ding, L., & Goshtasby, A. (2001). On the Canny edge detector. *Pattern Recognition*, *34*(3), 721–725. https://doi.org/10.1016/S0031-3203(00)00023-6

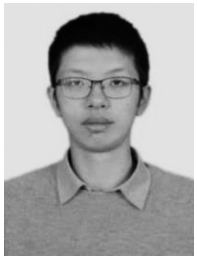

Dongxu Su obtained the B.Sc. degree (2016) from Sichuan University. He is currently a Ph.D. student at Xi'an Jiaotong University. His research activities focus on the machine tool spindle's thermal characteristics modelling and the measurement of the spindle error.

Xin Cai received B.Sc. degree from Dalian University of Technology, in 2019. At present, he is a student at the School of mechanical Engineering, Xi'an Jiaotong University. His research interests are thermal characteristic modeling and structure improvement of motorized spindle of CNC machine tools.

Yang Li received her Ph.D. degree in mechanical engineering from Xi'an Jiaotong University, Shaan xi, China. She is currently Assistant Professor. Her research is mainly about the compensation of the machine tool's thermal error.

Wanhua Zhao received Ph.D. degree from Xi'an Jiaotong University in 1998. He is currently one of Chair Professors of the Cheung Kong Scholars. He has authored or coauthored 2 books, over 50 journals. His current research interests include intelligent equipment theory and method based on deep learning.

Huijie Zhang received Ph.D. degree in mechanical engineering from Xi'an Jiaotong University, Shaan xi, China. He is currently an engineer at the Collaborative Innovation Center, Xi'an Jiaotong University. He is mainly responsible for helping students with the design and construction of their experimental platforms.